Smart Materials and Structures

Wet-adhesion properties of microstructured surfaces inspired by newt footpads

To cite this article before publication: Ling Gong *et al* 2018 *Smart Mater. Struct.* in press https://doi.org/10.1088/1361-665X/aad6d2

Wet-adhesion properties of microstructured surfaces inspired by newt footpads

Ling Gong[1,2], Haiwu Yu[2], Xuan Wu[2], Xiaojie Wang[*2]
[1]Department of Precision Machinery and Precision Instrumentation, University of Science and Technology of China, Hefei, Anhui 230026, People's Republic of China
[2]Institute of Advanced Manufacturing Technology, Hefei Institutes of Physical Science, Chinese Academy of Sciences, Changzhou, Jiangsu 213164, People's Republic of China

ABSTRACT

To understand wet adhesion of newt foot pads, we firstly examined and evaluated the attachment and climbing abilities of newts under three different wetting conditions. Then we characterized the micro and nanostructures of newts' foot pads by using the scanning electron microscopy (SEM). Followed by observing the micro and nanoscale structural features of newts' foot pads, four different micropatterns, including round pillars, hexagonal pillars, and two hybrid patterns with closed and semi-closed hexagonal ridges, were designed and fabricated on PDMS. The static friction and adhesion of microstructured surfaces were measured by using a multi-functional surface meter and an adhesion testing equipment, respectively. Effects of micropattern on static friction, and effects of retraction speed, amount of liquid, approach-retraction cycle on adhesion were investigated experimentally. Results suggested that a larger amount of liquid decreases the adhesion and friction, but a little liquid increases the adhesion and friction. It was found that there exists an optimum amount of liquid (about 0.1 μL) that can enhance the adhesion. Our results can give insights into the repeated shear movements of a newt's foot pads in the stream condition as well as the possible functions of dense nanopillar arrays on newt foot pads.

Keywords: Newts, Adhesive Pads, Microstructures, Biomimetics, Static Friction, Wet Adhesion

* xjwang@iamt.ac.cn

1. INTRODUCTION

In the last decades, biological adhesive systems have received lots of attention, because they can provide solutions to achieve highly adaptive and easily released synthetic adhesives. The adhesive pads of geckos, tree frogs and some other insects were found to show excellent attachment and detachment properties. They are reversible, reusable, self-cleaning and can work effectively even in wet surface conditions [1]. These features have triggered researchers' interests from different areas to understand the underlying mechanism for the development of bio-inspired adhesives. The bio-inspired adhesives have shown many applications such as in wall-climbing robots [2], novel grasping systems [3], biomedical devices [4,5], and automobile industry [6].

Biological adhesive systems in general can be classified into two categories according to their adhesive mechanisms: dry adhesion and wet adhesion. As a representative of the dry adhesion, the gecko's adhesive pads have attracted much attention. It was found that gecko's adhesive pads showed hierarchical surface construction (i.e., lamellae, setae and spatulae) on scales ranging from millimeters to nanometers [7]. The van der Waals forces were evidenced to be the dominant mechanism of dry adhesion [8]. However, the wet adhesion received relatively less attention as compared with the dry adhesion until recently. It is of great importance to develop bio-inspired adhesives that can be applied in wet environments.

As a representative of the wet adhesion, the tree frog's adhesive pads were studied [9,10]. It was found that the tree frog's toe pads consist of polygonal (largely hexagonal) epithelial cells that are separated by deep channels into which the mucous glands open. At nanoscale, the epithelial cell surface was further covered with dense nanopillar arrays. The surface tension (i.e. capillary force) of the liquid film was considered to be the primary mechanism of wet adhesion [11,12]. The toe-print examination [10] also illustrated the presence of fluid that surrounded each toe pad and filled the channels, indicating that the mucous liquid was a key in wet adhesion. However, Federle et al. [13] suggested that tree frogs can generate sufficient friction by bringing their toe pads into very close contact to the substrate surface. The two-level channels of toe pads most likely facilitate fast draining

of excess liquid between contact surfaces [6], whereas the micro- and nanostructures of the tree frog's toe pads were demonstrated to play an important role in friction enhancement [14]. In addition, the torrent and rock frogs [15,16] showed remarkable attachment abilities on the flooded surface due to the straight channels between epithelial cells.

Inspired by surface structures of tree frogs' adhesive pads, some synthetic adhesives were fabricated and the adhesion and friction properties were investigated. Drotlef et al. [17] systematically investigated the adhesion and friction properties of tree-frog-like patterns. They suggested that the surface structures of a tree frog's toe pads have been developed for climbing when shear forces involved. Wang et al. [18] investigated the influence of surface roughness on wet adhesion of man-made adhesive pads in mimicking tree frog toe pads and they found that the microstructures and preloads can significantly increase the wet adhesion if the profile height of the substrate surface is near or less than the width of microchannels in biomimetic adhesive pads. Varenberg and Gorb [19] experimentally confirmed that the hexagonal surface micropattern played a key role in wet adhesion enhancement. Tsipenyuk and Varenberg [20] suggested that the channel shape and contact area fraction of surface micropattern would affect the drainage rate of liquid, and consequently the friction in wet condition. Iturri et al. [21] and Chen et al. [5] found that the wet friction of the elongated hexagonal patterns depends on the sliding direction. Additionally, the wet adhesion of insect inspired microfiber arrays has also been investigated [22-24]. For example, Xue et al. [24] studied the insect inspired fibrillar adhesives that contained continuous pore systems and found that the synergistic interaction of capillarity and humidity-induced pad softening increases the pull-off force and the work of adhesion by two orders of magnitude.

Recently, one species (*Cynops orientalis*) of newt, an amphibian, has been found to possess superior sticking and climbing abilities in wet conditions [25,26]. The surface microstructure of newt toe pads plays an important role in friction enhancement for fast motion [27]. In order to further understand the wet adhesion of newts' foot pads, in this study, we firstly examined and evaluated the attachment and climbing abilities of newts under three different wetting conditions. Then we characterized the

micro and nanostructures of the adult and juvenile newts' foot pads by using the scanning electron microscopy (SEM). Followed by observing the micro and nanoscale structural features of newts' foot pads, four different micropatterns were fabricated on PDMS. The static friction and adhesion of microstructured surfaces were measured by using a multi-functional surface meter and an adhesion testing equipment, respectively. Effects of micropattern on static friction, and effects of retraction speed, amount of liquid, approach-retraction cycle on adhesion were investigated experimentally.

2. EXPERIMENTAL STUDY OF NEWTS

2.1 Attachment and climbing tests

Newts (*Cynops orientalis*) with a weight of about 1.0 g - 4.0 g and a total length of about 50 mm - 100 mm were purchased from a commercial supplier. They were fed in a water tank that contained stones and foliage. Dried mealworms were supplied every day. Fresh lake water was replaced each week. Only healthy and feeding newt individuals were used in experiments. This work was approved under protocol number SYXK (Wan) 2017-005.

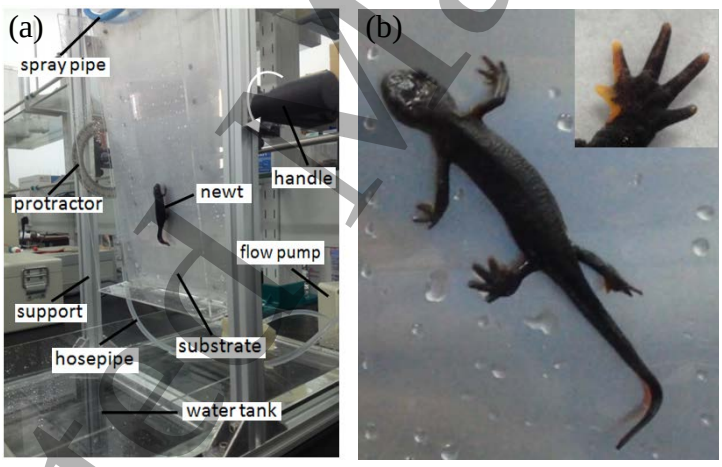

Fig. 1 (a) Tilting platform for newts attachment and climbing tests. (b) A newt (about 60 mm in length) used in tests and its left rear foot pad.

Thirteen and eleven newts were taken to conduct the attachment and climbing tests, respectively. A tilting platform was used for the tests as shown in figure 1. This platform could be manually rotated from 0º to 180º. The tilting angle of the platform was quantified via a 360° protractor. The water in

the tank was pumped along the hosepipe to the spray pipe that was fixed across the top end of the platform. The water poured out from small holes of the spray pipe to wet the substrate. In this study, a smooth Perspex sheet was used as the substrate material. The contact angle for the smooth Perspex sheet was about 70±5º [26], so the substrate could be wetted by water drops as shown in figure 1(b). Newts are native to mountain streams or ponds where the stream is not torrential. In whole animal trails, three wetting conditions were created by regulating flow rate of the flow pump: zero flow rate (0 mL/min) that modeled the dry condition, a low flow rate (50 mL/min) that modeled the wet condition, and a fast flow rate (120 mL/min) that modeled the stream condition.

The experimental conditions were set initially before each test. A newt was taken randomly from the tank and weighed. Then the newt was put on the substrate at a small tilting angle. For attachment tests, the platform was rotated slowly until the newt fell from the substrate; the angle of fall was recorded. For climbing tests, the platform was rotated slowly (the increment of angle is about 5 degree) to a specific tilting angle and held for about 30 s; by observation, if the newt was able to climb on such situation, the platform was rotated to a larger tilting angle and held again; the angle of climb was recorded when the newt's foot pads started sliding on the substrate. Each newt was tested 10 times for a specific experimental condition and given enough time (about 30 min) to recover between two trials.

Figure 2 shows the results of attachment and climbing tests, in which the fitting lines for a linear regression are also contained. The fitting and statistical analysis parameters (intercept, slope, degrees of freedom (DF), R^2 value, F-value and P-value) for the linear regression are listed in table 1. The decreasing trends of the fitting lines in figure 2(a) and 2(b) indicate that the angle of fall (fig. 2(a)) and angle of climb (fig. 2(b)) almost consistently decrease with newt body weight for all conditions. However, the P values (table 1) for climbing in the dry and stream conditions are very close to 0.05, which indicates that the dependence of angle of climb on newt body weight is weak under these conditions. Overall, the results show that the juvenile newts (with a weight of about 1.0 g - 2.0 g and a total length of about 50 mm - 60 mm) attach and climb better than the larger ones. The decrease of

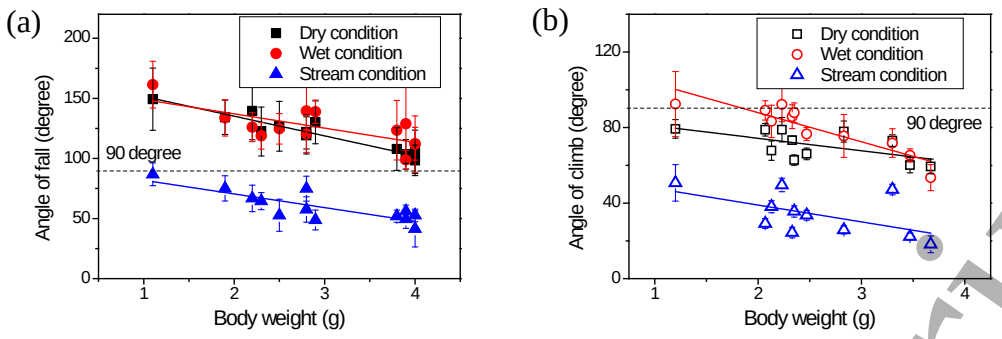

Fig. 2 Angle of fall (a) and angle of climb (b) of newts plotted against body weight under three different wetting conditions. Each data point is the average of 10 measurements and the error bars indicate the standard deviation. The black, red and blue lines of linear fitting correspond to different wetting conditions, respectively.

Table 1 The fitting and statistical analysis parameters for a linear regression

Category	Condition	Intercept	Slope	DF	R^2 value	F-value	P-value
Angle of fall	dry	168.03±4.742	-16.412±1.547	11	0.903	112.55	4.083e-7
	wet	160.899±10.696	-11.884±3.489	11	0.469	11.6	0.00587
	stream	93.269±7.284	-11.391±2.376	11	0.647	22.981	5.588e-4
Angle of climb	dry	87.549±7.537	-6.611±2.854	9	0.304	5.365	0.04577
	wet	118.731±6.468	-15.421±2.449	9	0.794	39.635	1.417e-4
	stream	56.754±11.457	-8.898±4.339	9	0.243	4.205	0.07054

weight-specific attachment and climbing is most likely due to smaller surface to volume ratio [28]. Under both dry and wet conditions, the angle of fall is greater than 90° for all newts. The juvenile newts could attach in an upside down position in some cases. Though the angle of climb is clearly lower than the angle of fall under all conditions, the juvenile newts were still able to climb on the almost vertical substrate surface in the wet condition. For the attachment, the fitting parameters of the intercept as well as the slope (table 1) in the dry condition are not very statistically different with

that of the wet condition, but for the climbing, they are different. The angle of fall and angle of climb seem to be slightly higher for the wet condition compared to the dry condition (see regression lines in fig. 2), which implies that a little water on the substrate may be helpful for the attachment and climbing of newts. Under the stream condition, however, the angle of fall and angle of climb decrease remarkably (see regression lines in fig. 2). The repeated shear movements (i.e., sliding, peeling and repositioning actions) of foot pads were commonly observed. This is because that the stream tends to break the integrity of meniscus between foot pads and the substrate surface, and that a thick layer of liquid film in the contact zone would significantly decrease both adhesion and friction forces of foot pads. The wettability of a substrate can influence not only the adhesion but also the friction of a live animal [29]. The decrease of the angle of fall and angle of climb in the stream condition comparing with the dry and wet conditions is possibly due to the wettable property of the Perspex substrate surface.

2.2 Microstructure characterization of foot pads

The scanning electron microscopy (SEM) was used to study surface micro- and nanostructures of newts' foot pads. Newts were given a lethal dose of Benzocaine. Fore- and hindlimbs of the newts were excised with a scissor. The tissue samples were immediately fixed in 2.5% glutaraldehyde in 0.1 M phosphate buffer for 24 h. Then they were rinsed three times (15 min per rinse) in 0.1 M phosphate buffer (PH, 7.2). After that, the tissue samples were post-fixed in 1% osmium tetroxide in 0.1 M phosphate buffer for 2 h - 3 h, and rinsed again. The fixed samples were dehydrated through an alcohol series (70%, 80%, 90%, 95% and 100%, 24 h in each). Then the samples were critical point dried, mounted, sputter-coated, and viewed on a JSM-6360LA SEM at an operating voltage of 15 KV.

Figure 3 shows the scanning electron micrographs of newts' foot pads. It was observed that there are narrow channels (arrows in fig. 3(a)) between polygonal epithelial cells for the adult newt (with a weight of about 4.0 g and a total length of about 100 mm) (fig. 3(a)). In contrast, the micro-ridge (arrows in fig. 3(b), about 180 nm in height and 340 nm in width [25]) networks that surround

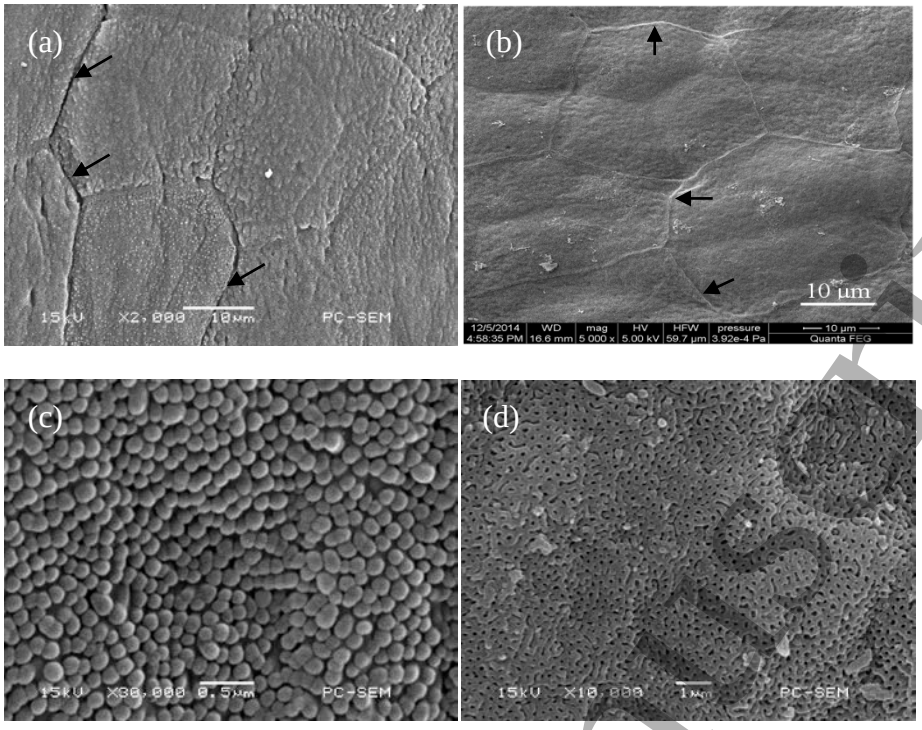

Fig. 3 Scanning electron micrographs of newts' foot pads. (a) Narrow channels (arrows) between epithelial cells for the adult newt. (b) Micro-ridge networks (arrows) surrounding epithelial cells for the juvenile newt. (c) The epithelial cell surface is covered with a dense array of nanopillars for both adult and juvenile newts. (d) The dorsal surface and outside of foot pad are covered with porous networks for both adult and juvenile newts.

polygonal epithelial cells were observed for the juvenile newt (fig. 3(b)). Similar structural features were observed on a tree frog's toe pads in its different development stages [30]. The narrow channels that separate epithelial cells may function to evenly spread the mucus over the foot pad surface and drain excess liquid underneath the foot pad. The micro-ridge networks may function to enhance the shear resistance of foot pads by mechanical locking with microscale asperities of the substrate surface. At nanoscale, the polygonal epithelial cell surface of foot pads is covered with a dense array of nanopillars for the adult and juvenile newts (fig. 3(c)). The nanopillars were surrounded by smaller channels and each nanopillar (about 160 nm in height and width) has a semi-spherical tip [25]. The dense nanopillar arrays may play an important role in the attachment and climbing of

newts, since they come into direct contact with substrate surfaces. The dorsal surface and outside of the foot pad instead are covered with porous networks for the adult and juvenile newts (fig. 3(d)), indicating that the foot pads are the main functional zones of attachment and climbing.

3. EXPERIMENTAL STUDY OF MICROSTRUCTURED SURFACES

3.1 Design and fabrication

The juvenile newts showed superior attachment and climbing performance (fig. 2), which should be closely related to the micro- and nanostructures on their footpads, such as micro-ridge networks (fig. 3(b)), dense nanopillar arrays (fig. 3(c)). Inspired by the surface structures, a hybrid pattern of round pillars surrounded by a closed hexagonal ridge (fig. 4(c)) was designed. Considering the important role of narrow channels in drainage (fig. 3(a)), a similar hybrid pattern with a semi-closed hexagonal ridge (fig. 4(d)) also was designed. In addition, round (fig. 4(a)) and hexagonal (fig. 4(b)) pillars that have been mostly studied were chosen to compare with the hybrid patterns. For these four different patterns in figure 4, the corresponding area ratio (r) that is defined as the ratio of the top area of microstructures over the whole pattern area can be calculated as follows:

$$r_{\text{round}} = \frac{\pi d^2}{2\sqrt{3}L^2} \quad (1)$$

$$r_{\text{hexagonal}} = \frac{3d^2}{4L^2} \quad (2)$$

$$r_{\text{closed}} = 1 - \frac{9D^2 - 2\sqrt{3}\pi n d^2}{(3D + 4\sqrt{3}H)^2} \quad (3)$$

$$r_{\text{semi-closed}} = 1 - \frac{9D^2 + 48\sqrt{3}BH - 2\sqrt{3}\pi n d^2}{(3D + 4\sqrt{3}H)^2} \quad (4)$$

where d denotes the diameter of round pillar or the circumscribed circle diameter of hexagonal pillar, L the distance between two adjacent pillars, H the width of hexagonal ridge, D the circumscribed circle diameter of the inner wall of hexagonal ridge, B the split width of the semi-closed hexagonal ridge, and n the number of round pillars surrounded by a hexagonal ridge. In the present study, the following design parameters are used:

round pillars, d=150 μm, L: 200~450 μm;

hexagonal pillars, d=100/200 μm, L: 120~550 μm;

closed hexagonal ridge, H=50 μm, D=500 μm, d=50 μm, n: 7~37;

semi-closed hexagonal ridge, H=50 μm, D=500 μm, B=100 μm, d=50 μm, n: 7~37.

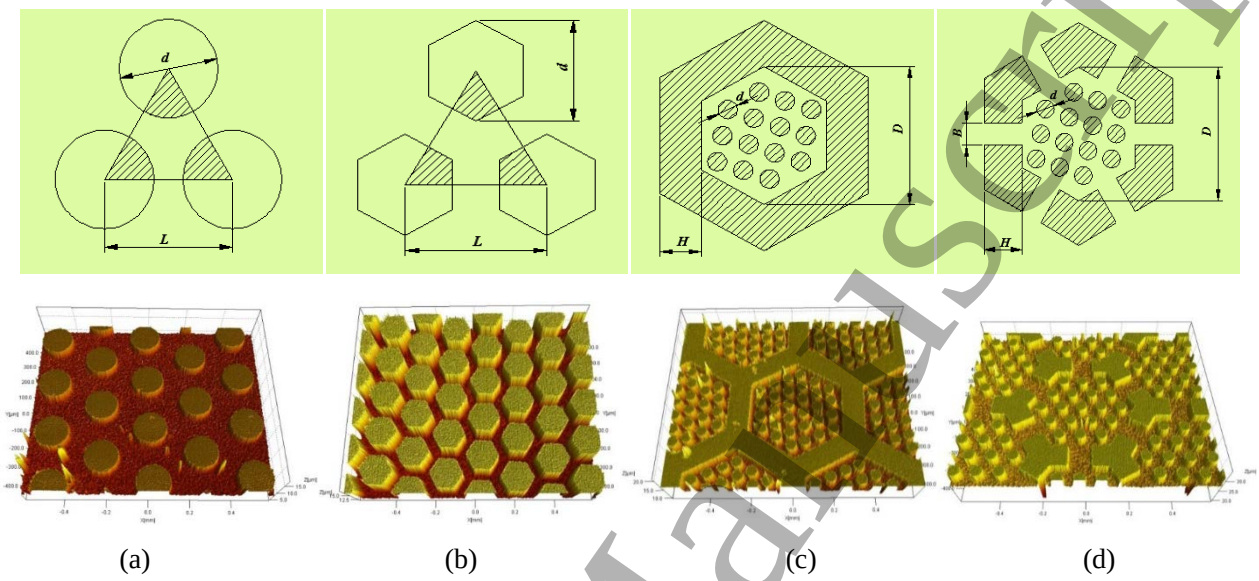

(a) (b) (c) (d)

Fig. 4 Four different micropatterns and the corresponding 3D profiles. (a) Round pillars. (b) Hexagonal pillars. Round pillars surrounded by a closed (c) and a semi-closed (d) hexagonal ridges.

The commercially available polydimethylsiloxane (PDMS) (Dow Corning, Midland, MI, USA) was used to fabricate samples with different microstructured surfaces by lithography and replica techniques. The fabrication procedures were as follows: (1) a photoresist was spin coated onto a clean glass substrate to produce an uniform layer of 5±0.2 μm thickness; (2) an inverse mold was produced on the coated surface by contact photolithography; (3) the PDMS solution (prepolymer and curing agent mixed by a weight ratio of 10:1) was poured into the inverse mold; (4) the PDMS sample was peeled off the mold after curing. Figure 4 shows three-dimensional (3D) profiles of different microstructured surfaces.

3.2 Equipment and measurement procedures

3.2.1 Contact angle measurements

The contact angle measurement setup (SL200B, Shanghai Solon Information Technology Co. LTD) was used to study the wettability of different microstructured surfaces. The setup is based on the method of standard image analysis. By means of the pipette, a drop of deionized water (3 μL) is put on the microstructured surface under investigation. A CCD camera images the profile of the drop. The contact angle is measured by θ/2 method based on the image processing software CAST2.0. The contact angle and the work of adhesion between the drop and the surface are obtained from the measurements. The measuring range of the setup is from 3° to 180°. The resolution is 0.01°, and the precision is ±2°. At least three measurements were conducted at different positions of the same microstructured surface and the results were averaged. All measurements were conducted at room temperature and normal atmosphere.

3.2.2 Static friction measurements

The static friction measurements were carried out on a multi-functional surface meter TYPE32 (fig. 5(a)). The upper specimen is a 10 mm-diameter bearing steel sphere, and the lower specimen is the PDMS sample. The PDMS sample is fixed on the mobile platform of the equipment. For each test, the upper specimen was brought into contact with the lower PDMS sample; the friction force were continuously recorded with the contact tribopair relatively slipping a displacement of 3 mm at a speed of 100 μm/s. PDMS samples with four different microstructured surfaces (fig. 4) were measured under the dry and wet conditions. In the wet condition, 30 μL water was added by using a micropipette to model an experimental condition of larger amount of liquid that approximately corresponds to the stream condition used in whole animal trails. The normal force is fixed at 100 g weight. At least three measurements were conducted at different positions of the microstructured surface for a specific experimental condition and the results were averaged. Figure 5(b) shows a typical friction force curve, from which the static friction force is extracted and the static coefficient of friction is calculated with the known normal force.

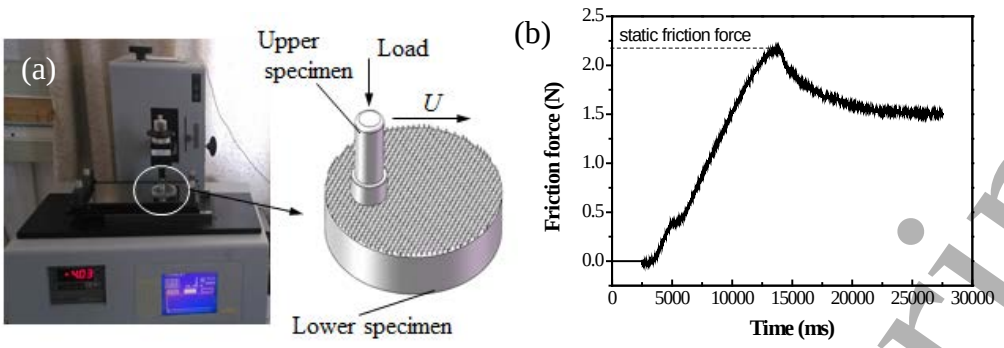

Fig. 5 (a) The equipment for static friction measurements and the tribopair. (b) A typical friction force curve.

3.2.3 Adhesion measurements

The adhesion of PDMS samples were measured on a homebuilt testing equipment (fig. 6(a)). A flat cylindrical glass of 10 mm diameter was used as the indenter. The contact angle for the smooth glass was about 35±5º [26]. The glass indenter was attached to the force sensor (2.2 lb, LRF 400, Futek, Irvine, CA, USA) that was mounted on a *z*-translation stage (T-LSM 050B, Zaber Tech, British Columbia, Canada). The PDMS sample was fixed on the specimen stage. A certain amount of liquid (fresh water) was added to the contact zone by using a micropipette. In a typical test, the indenter was brought into contact with the PDMS sample. After an indentation displacement was reached and the system was stable, the indenter retracted at a specific speed and finally pulled off the sample. Force data throughout the test were continuously recorded via a data acquisition unit (IHH 500, Futek, Irvine, CA, USA). Microstructured surfaces containing the hybrid pattern (fig. 4(c)) that is composed of round pillars surrounded by a closed hexagonal ridge were measured. Three area ratios of round pillars ($r_1 = 2\sqrt{3}n\pi d^2/(3D + 4\sqrt{3}H)^2$, where n is the number of round pillars) (5.59%, 11.17%, and 23.94%) were used. One should notice that the area ratio here does not contain that of the closed hexagonal ridge ($r_2 = 1 - 9D^2/(3D + 4\sqrt{3}H)^2$) (34%) of the hybrid pattern (fig. 4(c)).

Effects of retraction speed, amount of liquid and approach-retraction cycle on the adhesion were evaluated. For the measurements of retraction speed effect, the indenter approached the sample at 10

μm/s until the displacement of 200 μm was reached, then retracted at different speeds (changing from 5 μm/s to 200 μm/s). Both dry and wet (0.1 μL water) conditions were considered in the study. For the measurements of effect of amount of liquid, different amounts of liquid (changing from 0 μL to 10 μL) were added to the contact zone at the beginning of each test. The approach speed, indentation displacement and retraction speed were fixed at 10 μm/s, 200 μm, and 10 μm/s, respectively. For a certain amount of liquid, the approach-retraction process was conducted sequentially to study the effect of approach-retraction cycle. A set of tests were conducted at the same position of the microstructured surface. Figure 6(b) shows a typical force curve, in which the pull-off force (i.e., adhesion force) is defined as the peak tensile force during retraction.

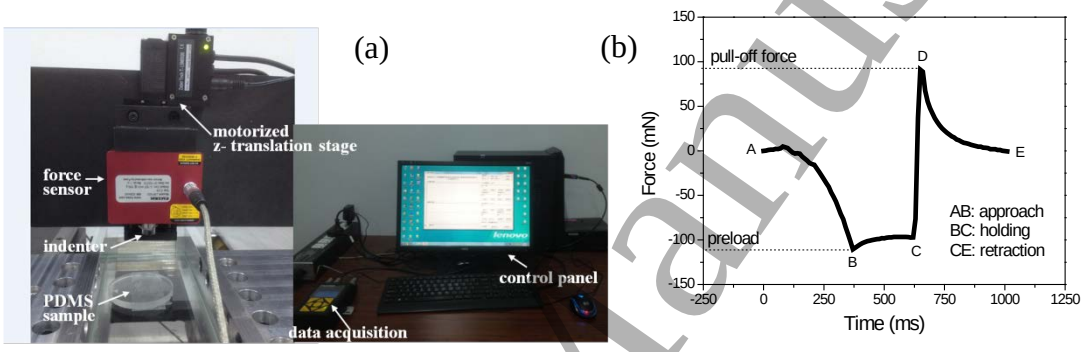

Fig. 6 (a) The equipment for adhesion measurements. (b) A typical force curve showing the experimental procedures, in which the pull-off force is defined.

3.3 Results and Discussion

3.3.1 Contact angle measurements

Figure 7 shows results of static contact angle measurements for different microstructured surfaces. The contact angle is larger than 90º for all PDMS samples with different microstructured surfaces (fig. 7(a)), indicating that the microstructured surfaces are hydrophobic. Among four different micropatterns, the hybrid pattern with a closed hexagonal ridge shows a gradually decreasing contact angle with the increasing pillar area ratio. Meanwhile, the work of adhesion between the drop of water and the hybrid pattern accordingly increases (fig. 7(b)). The work of adhesion was given directly by the contact angle measurements of the system, which can be calculated according to the

equation: $W_a = \gamma_{gl}(1 + \cos\theta)$, where W_a denotes the work of adhesion, γ_{gl} the surface tension of liquid (72.8 mN/m), and θ the measured mean contact angle.

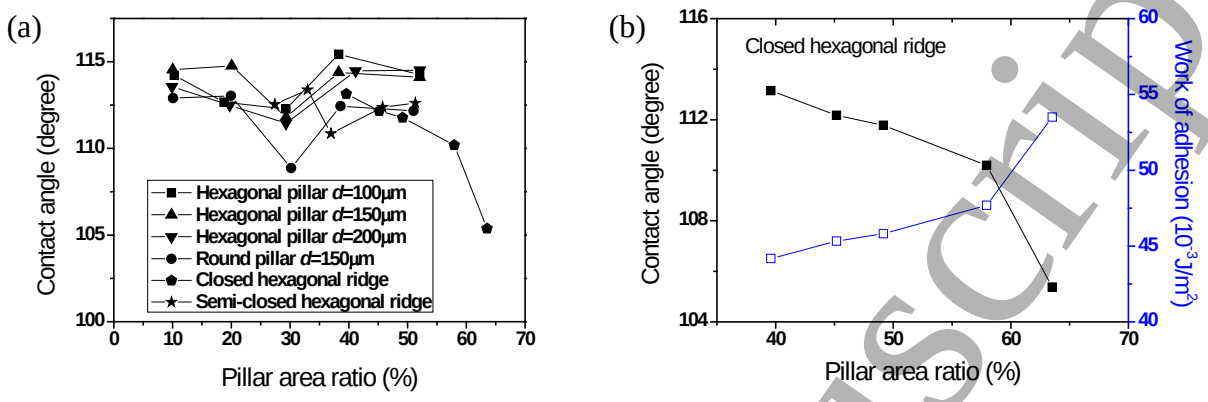

Fig. 7 (a) Contact angle plotted against pillar area ratio for different microstructured surfaces. (b) Contact angle and work of adhesion for the hybrid pattern with a closed hexagonal ridge plotted versus pillar area ratio.

3.3.2 Static friction measurements

Effect of micropattern

As shown in figure 8, the static coefficient of friction for different microstructured surfaces almost consistently increases with the pillar area ratio. The addition of 30 μL water decreases the static friction compared to the dry condition, which is consistent with the results of attachment and climbing tests of newts where the angle of fall and angle of climb remarkably decrease for the stream condition (fig. 2). The liquid affected the direct solid-solid contact interaction between the upper and lower specimens maybe by introducing the boundary lubrication effect.

The static coefficient of friction for hexagonal pillars increases with the decreasing pillar diameter under different wetting conditions. So the hexagonal pillars with pillar diameter of 100 μm showed better static friction in both dry and wet conditions (fig. 8(a)). The hexagonal pillars also showed better static friction as compared with the round pillars. In comparison with the hexagonal pillars with pillar diameter of 100 μm, the hybrid patterns with a closed and a semi-closed hexagonal ridges

show a faster increasing static friction with the pillar area ratio (fig. 8(b)). When the pillar area ratio is large enough, the static friction of the hybrid patterns approaches and even surpasses that of the hexagonal pillars. The faster increase and comparable static friction should be related to the smaller diameter (d=50 μm) of round pillars surrounded by the hexagonal ridge. More pillars would be in contact with the flat indenter for a larger pillar area ratio and a smaller pillar diameter; the adhesion enhanced friction effect may be more significant in terms of the contact splitting mechanism [31]. What's more, the network structures constructed by the closed and semi-closed hexagonal ridges may also contribute to the enhancement of static friction. Iturri et al. [21] suggested that the edge density of the pattern is a key factor in the friction enhancement. In comparison with the hybrid pattern with a closed hexagonal ridge, the hybrid pattern with a semi-closed hexagonal ridge shows better static friction in the wet condition (fig. 8(b)). This is because that the semi-closed hexagonal ridge can facilitate the drainage of excess liquid in the contact zone. The decrease of coefficient of friction for the closed hexagonal ridge (fig. 8(b)) may be related to distinct properties at different positions of the sample surface. The significant standard deviation shown in figure 8(b) also indicates this.

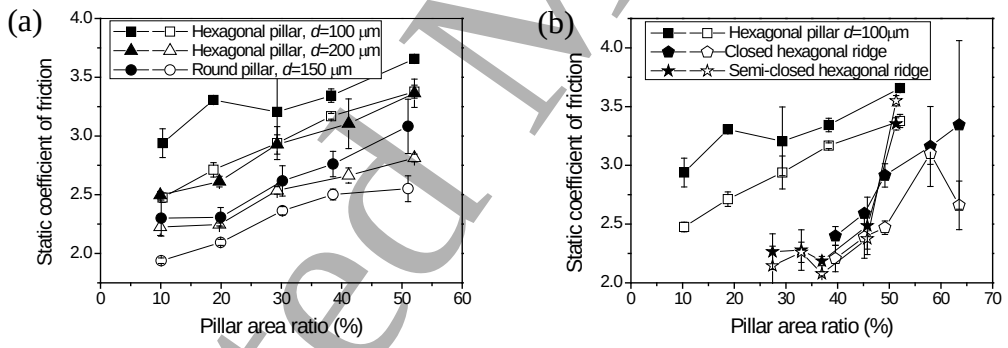

Fig. 8 Static coefficient of friction plotted against pillar area ratio for different microstructured surfaces under dry (filled data marker) and wet (30 μL water) (empty data marker) conditions. (a) Hexagonal and round pillars. (b) Hexagonal pillars and hybrid patterns. The error bars indicate the standard deviation.

The results indicate that the tip shape and size of micropillar, and the draining channel have

significant influence on the static friction of microstructured surfaces. Among four different micropatterns, the hexagonal pillars showed more stable static friction under both dry and wet conditions. This finding is consistent with Varenberg and Gorb's [19] and Tsipenyuk and Varenberg's work [20], in which they found that the hexagonal surface texture is much more effective in the drainage of fluid. However, one must notice that the hybrid patterns, especially the semi-closed one, showed the potential to fast increase the static friction for a larger pillar area ratio and a smaller pillar diameter. We speculate that the dense nanopillar arrays on newts' footpads must represent a type of naturally optimized structures that can cope with different environmental conditions.

3.3.3 Adhesion measurements

Effect of retraction speed

As shown in figure 9(a), the pull-off force increases with the retraction speed for both dry and wet conditions. This is because that the retraction speed and viscoelastic deformation of PDMS samples can cause the effective work of adhesion to increase [32]. Figure 9(b) shows magnified data points enclosed in the black box in figure 9(a). One can see that when the retraction speed is relatively low (≤50 μm/s), the pull-off force is consistently larger in the wet condition compared to the dry condition for different pillar area ratios. However, at higher retraction speeds (i.e., 100 μm/s and 200 μm/s), the pull-off force tends to be lower in the wet condition (fig. 9(a)). The speed dependence is most likely related to the formation of meniscus between the flat indenter and the microstructured surface. There is enough time to form the meniscus for a low retraction speed. So the meniscus force leads to the increase of pull-off force. However, a higher retraction speed possibly limits the formation of meniscus. The thin liquid film trapped in the contact zone that does not respond immediately to the retraction speed weakens the direct interactions between the indenter and the microstructured surface. In the attachment and climbing tests of newts, we observed that newts crawled more carefully and slowly on a wet and inclined (about 90^{o}) substrate surface (not shown). Based on the present results (fig. 9), we speculate that newts also need some time to build a stable attachment state among footpads, the liquid film and the substrate surface before taking a step forward.

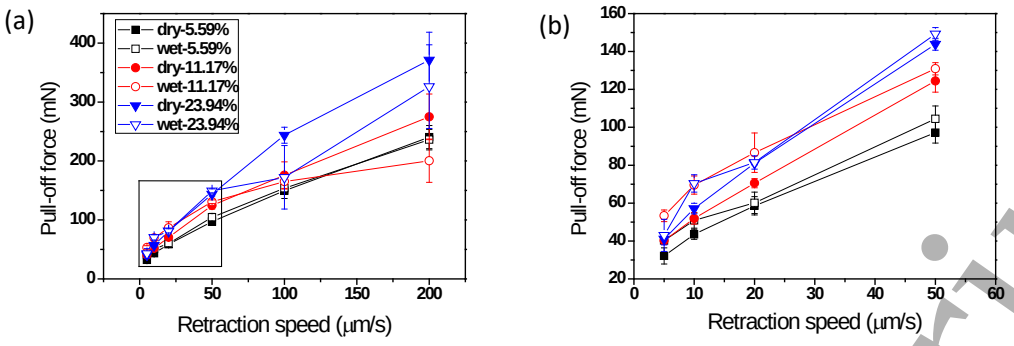

Fig. 9 (a) Pull-off force plotted against retraction speed under dry and wet (0.1 μL water) conditions for different pillar area ratios. (b) Magnification of data points in the black box in figure 9(a). The error bars in figures represent the standard deviation.

Effect of amount of liquid

Figure 10 shows that a very small amount of liquid (about 0.1 μL) tends to increase the pull-off force compared to the dry condition (0 μL), which is consistent with the results of retraction speed effect in figure 9(b). Then the pull-off force decreases with the increasing amount of liquid. However, the pull-off force does not decrease consistently with the further increasing amount of liquid, but shows a fluctuation. Additionally, we extracted the duration from the peak tensile force to the zero force (i.e., DE segment in figure 6(b)). Figure 11(a) shows that the duration increases with the increasing amount of liquid, which indicates that the direct contact interaction (0 μL) between the microstructured surface and the flat indenter would be replaced by the interaction (>0 μL) among the microstructured surface, liquid film and the flat indenter.

The results suggest that there exists an optimum amount of liquid (about 0.1 μL) that can enhance the pull-off force, which can be used to account for that newts attach and climb relatively better in the wet condition compared to the dry condition (fig. 2). A thin liquid film trapped in the contact zone may enhance newts' attachment and climbing performance. One should notice that the substrates used in biological and bio-inspired tests are different. As the wettability of a substrate affects the adhesion differently [29], the comparisons across experiments may not make strong connections between the whole animal performance and the synthetic performance. Then the pull-off

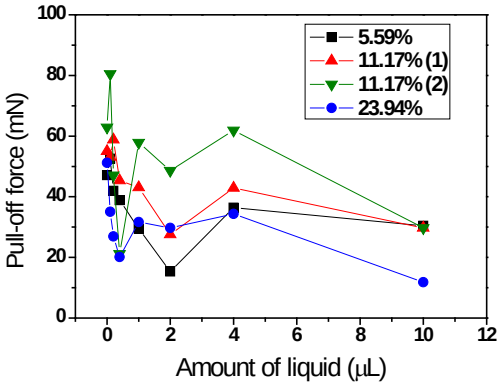

Fig. 10 Effect of amount of liquid on pull-off force for different pillar area ratios. The markers (1) and (2) represent measurement results from two different positions.

force decreases with increasing amount of liquid, which agrees with the adhesion mechanism based on capillary forces [33]. A decrease in the adhesion force caused by increasing liquid volume was reported for hydrophilic microstructured surfaces [17]. Defante et al. [34] observed that the interstitial water at the contact interface between hydrophobic PDMS and PVNODC (a polymer coating) leads to a reduction in adhesion compared to the dry contact. Similar phenomena were observed for hydrophobic microstructured surfaces (fig. 7(b)) used in this study, even though that capillary forces were suggested [17,35] to only make a small contribution to adhesion force. This is possibly related to the hybrid structure with a closed hexagonal ridge (fig. 4(c)) as well as the size (d=10 mm) and the hydrophilic surface of glass indenter used in adhesion measurements. In the attachment and climbing tests of newts (fig. 2), the stream condition remarkably decreased the attachment and climbing performance of newts due to the integrity of meniscus being broken and a thick layer of liquid film in the contact zone significantly decreasing the adhesion and friction forces of foot pads. The pull-off force does not consistently decrease with the further increasing amount of liquid. This inconsistence may be related to hydrodynamic effect, which can be enhanced due to the compliant material property of PDMS samples [36]. Dhong and Frechette [37] investigated the coupled effects of applied load and surface structure on the viscous forces during peeling and they observed three regimes based on hydrodynamics, in which the work of separation depends on the

fluid film thickness prior to pull out.

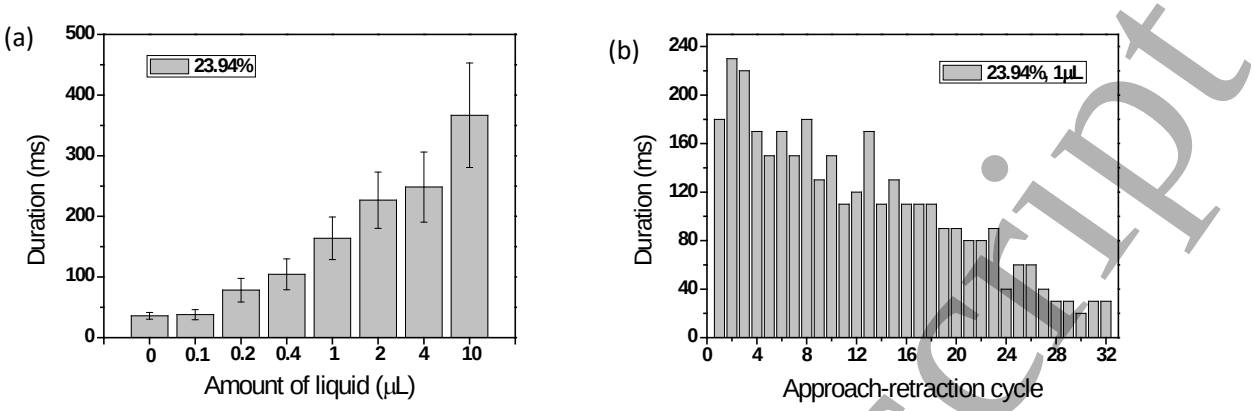

Fig. 11 Duration plotted against amount of liquid (a) and approach-retraction cycle for the microstructured surface with 23.94% pillar area ratio. The error bars in figure (a) represent the standard deviation.

Effect of approach-retraction cycle

To model consecutive steps of newts and study the durability of liquid film, the approach-retraction cycle experiments were conducted while keeping the indenter at the same position of the microstructured surface. As shown in figure 12, the first approach-retraction cycle in general corresponds to a relatively high pull-off force. Then the pull-off force decreases to a lower level starting from the second cycle. After a certain number of approach-retraction cycles, the pull-off force increases to a higher level and then seems to show a decreasing trend (arrows in fig. 12(a)-12(c)). The liquid film between the indenter and the PDMS sample should be thicker for a larger amount of liquid (fig. 12(a)-12(c)), so more approach-retraction cycles are needed to thin the liquid film.

At the beginning of the first approach-retraction cycle test, a certain amount of liquid was added to the flat indenter surface, so the microstructured surface is not contaminated with the liquid. At the end of the first approach-retraction cycle, the liquid on the indenter surface is redistributed to the microstructured surface after rupture of the liquid bridges. The results indicate that an intact liquid configuration appears to benefit the wet adhesion. During consecutive approach-retraction cycles,

the liquid in the contact zone is reduced gradually by being squeezed out of the contact zone and evaporated, and finally the liquid will be depleted. Figure 11(b) shows that the duration decreases gradually with the sequential approach-retraction cycle, which corresponds to the reduction of the amount of liquid. When the amount of liquid trapped in the contact zone reduces to the optimum level (about 0.1 μL), the enhanced meniscus force leads to the increase of the pull-off force. The decreasing trend of pull-off force should be related to the further reduction of amount of liquid. It should be noted that the direct contact force may also contribute to the adhesion when the liquid film is thin enough (<10 nm).

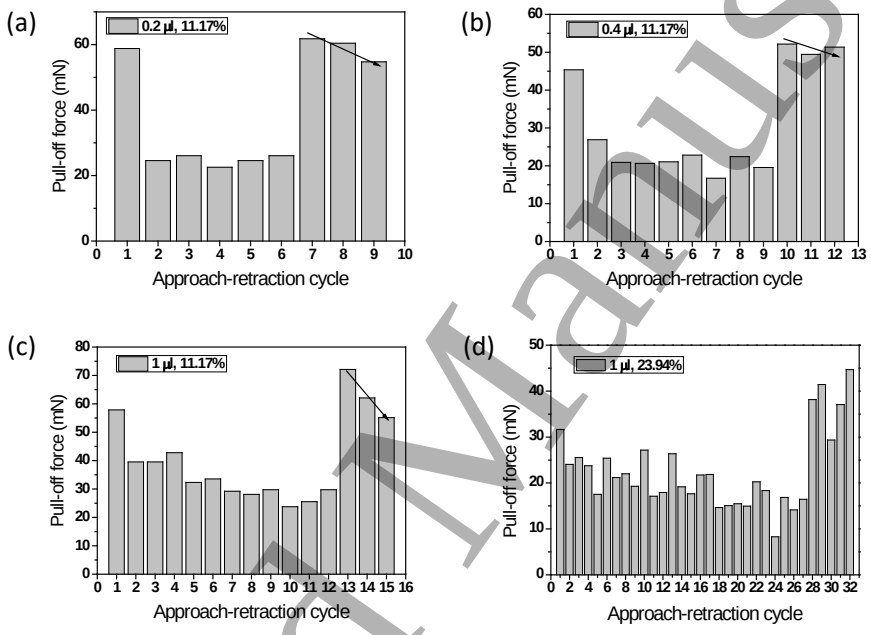

Fig. 12 Effect of approach-retraction cycle on pull-off force for different amounts of liquid and pillar area ratios. (a) 0.2 μL, 11.17%; (b) 0.4 μL, 11.17%; (c) 1 μL, 11.17%; (d) 1 μL, 23.94%. Black arrows in figures indicate the decreasing trend.

The results can provide insights into the repeated shear movements of a newt's foot pads. When a newt climbs on an inclined surface that is wetted by water, the pads are prone to encounter big drops of water or even be submerged in the water. The repeated shear movements of pads are observed because a thick layer of water film that separates the pads and the substrate significantly decreases

both adhesion and friction forces (fig. 2). Combining repeated sliding, peeling and repositioning actions of foot pads, as well as the compliant property of foot pads (about 560 kPa [25]) and draining channels on foot pads (fig. 3), the water film can be thinned effectively. The pads stop sliding until enough forces (meniscus and/or direct contact forces) are produced to resist against the shear movements.

For the same amount of liquid (fig. 12(c) and 12(d)), the microstructured surface with a larger area ratio of round pillars (23.94%) needs more approach-retraction cycles to thin the liquid film and thus to increase the pull-off force, which implies that a finer microstructure can keep the liquid around the round pillars from being fast squeezed out and evaporated. Similarly, the numerical study demonstrated that an increase in the density of the substrate structures causes more fluid adsorbed [38]. The underlying mechanism may involve anchorage of narrow channels to the liquid [39]. Figure 7(b) shows that the work of adhesion between the drop of water and the microstructured surface increases with the pillar area ratio. For a finer microstructure, the work of adhesion is larger, so the attachment between the drop and the microstructured surface should be stronger.

Recall that the epithelial cell surface of newt foot pads is covered with a dense array of nanopillars that are separated each other by small channels (fig. 3(c)). We speculate that the small channels around each nanopillar may function as a reservoir of secretion, which can effectively protect the secretion from being fast depleted due to deposition on substrates and evaporation. In addition, the small channels may also facilitate fast drainage of excess water to increase close contacts when newts climb in wet environments, which is similar to the function of small channels on a tree frog's toe pads [6,9]. Therefore, the dense nanopillar arrays on newt foot pads are evolved possibly to retain significant adhesion and friction even in the presence of liquid.

4. CONCLUSIONS

In this study, we examined the attachment and climbing abilities of newts and studied the micro and nanoscale structural features of newt foot pads. The results indicated that the juvenile newts had

better attachment and climbing performance in wet environments. The addition of a little water seems to benefit the enhancement of the attachment and climbing abilities of newts. However, the stream condition remarkably decreases the attachment and climbing abilities of newts due to the integrity of the meniscus being broken.

Inspired by surface structures of newt foot pads, four different micropatterns, including round pillars, hexagonal pillars, and two hybrid patterns with closed and semi-closed hexagonal ridges, were fabricated on PDMS. Both the static friction and adhesion of microstructured surfaces were investigated under dry and wet conditions. In the static friction tests, the results indicated that the tip shape and size of micropillar, and the draining channel had significant influence on the friction in wet condition. The pattern of hexagonal pillars showed more stable static friction under both dry and wet conditions. The hybrid patterns, especially the semi-closed one, showed the potential to fast increase the static friction for a larger pillar area ratio and a smaller pillar diameter. In the adhesion tests, the results indicated that the pull-off force depends on the retraction speed. The pull-off force in wet condition is larger than that in dry condition for a low retraction speed ($\leq$50 μm/s). However, the pull-off force tends to be lower in wet condition compared to dry condition for a higher retraction speed. It was found that there exists an optimum amount of liquid (about 0.1 μL) that can enhance the adhesion. When the amount of liquid decreases to the optimum level with sequential approach-retraction cycles, the pull-off force increases. This provides insights into the shear movements of a newt's foot pads in the stream condition that they effectively thin the thick water film between contact surfaces to enhance shear resistance by repeated sliding, peeling and repositioning actions of foot pads. A finer microstructure seems to be able to preserve the liquid around the pillars for a longer time, which implies that the dense nanopillar arrays on newts' foot pads may have the function to keep foot pads wet to retain significant adhesion and friction.

ACKNOWLEDGES

The authors would like to thank Rong Li and Hongduo Jia from the Institute of Advanced Manufacturing Technology for their assistance in experimental studies. This work is financially

supported by the National Natural Science Foundation of China (grant no. 51305425, and 51605467) and Youth Innovation Promotion Association CAS (NO: 2016387).

REFERENCES

[1] Favi P M, Yi S, Lenaghan S C, Xia L and Zhang M 2014 Inspiration from the natural world: from bio-adhesives to bio-inspired adhesives *J. Adhes. Sci. Technol.* 28 290–319

[2] Li M, He B, Qin H, Zhou Y, Lu H and Yue J 2011 A wet adhesion inspired biomimetic pad with direction dependence and adaptability *Chinese Sci. Bull.* 56 1935–41

[3] Zhou M, Tian Y, Sameoto D, Zhang X, Meng Y and Wen S 2013 Controllable Interfacial Adhesion Applied to Transfer Light and Fragile Objects by Using Gecko Inspired Mushroom-Shaped Pillar Surface *ACS Appl. Mater. Interfaces* 5 10137–44

[4] Roshan R, Jayne D G, Liskiewicz T, Taylor G W, Gaskell P H, Chen L, Montellano-Lopez A, Morina A and Neville A 2011 Effect of tribological factors on wet adhesion of a microstructured surface to peritoneal tissue *Acta Biomaterialia* 7 4007–17

[5] Chen H, Zhang L, Zhang D, Zhang P and Han Z 2015 Bioinspired surface for surgical graspers based on the strong wet friction of tree frog toe pads *Appl. Mater. Interfaces* 7 13987–95

[6] Persson B N J 2007 Wet adhesion with application to tree frog adhesive toe pads and tires *J. Phys-Condens. Mat.* 19 376110

[7] Bhushan B 2007 Adhesion of multi-level hierarchical attachment systems in gecko feet *J. Adhes. Sci. Technol.* 21 1213–58

[8] Autumn K and Peattie A M 2002 Mechanisms of adhesion in geckos *Integr. Comp. Biol.* 42 1081–90

[9] Scholz I, Barnes W J, Smith J M and Baumgartner W 2009 Ultrastructure and physical properties of an adhesive surface, the toe pad epithelium of the tree frog, Litoria caerulea White *J. Exp. Biol.* 212 155–62

[10] Barnes W J, Baum M, Peisker H and Gorb S N 2013 Comparative Cryo-SEM and AFM

studies of hylid and rhacophorid tree frog toe pads *J. Morphol*. 274 1384–96

[11] Emerson S B and Diehl D 1980 Toe pad morphology and mechanisms of sticking in frogs *Biol. J. Linn. Soc.* 13 199–216

[12] Hanna G and Barnes W J 1991 Adhesion and detachment of the toe pads of tree frogs *J. Exp. Biol.* 155 103–25

[13] Federle W, Barnes W J, Baumgartner W, Drechsler P and Smith J M 2006 Wet but not slippery: Boundary friction in tree frog adhesive toe pads *J. R. Soc. Interface* 3 689–97

[14] Kappl M, Kaveh F and Barnes W J 2016 Nanoscale friction and adhesion of tree frog toe pads *Bioinspir. Biomim.* 11 035003

[15] Drotlef D M, Appel E, Peisker H, Dening K ,der Campo A, Gorb S N and Barnes W J P 2015 Morphological studies of the toe pads of the rock frog, Staurois parvus (family: Ranidae) and their relevance to the development of new biomimetically inspired reversible adhesives *Interface Focus* 5 20140036

[16] Endlein T, Barnes W J P, Samuel D S, Crawford N A, Biaw A B and Grafe U 2013 Sticking under wet conditions: the remarkable attachment abilities of the torrent frog, Staurois guttatus *PloS one* 8 e73810

[17] Drotlef D M, Stepien L, Kappl M, Barnes W J P, Butt H J and der Campo A 2013 Biomimetics: Insights into the adhesive mechanisms of tree frogs using artificial mimics *Adv. Funct. Mater.* 23 1137–46

[18] Wang K, He B and Shen R J 2012 Influence of surface roughness on wet adhesion of biomimetic adhesive pads with planar microstructures *Micro & Nano Letters* 7 1274–7

[19] Varenberg M and Gorb S N 2009 Hexagonal surface micropattern for dry and wet friction *Advanced Materials* 21 483–6

[20] Tsipenyuk A and Varenberg M 2014 Use of biomimetic hexagonal surface texture in friction against lubricated skin *J. R. Soc. Interface* 11 20140113

[21] Iturri J, Xue L, Kappl M, García-Fernández L, Barnes W J P, Butt H J and der Campo A 2015 Wet Adhesion: Torrent Frog-Inspired Adhesives: Attachment to Flooded Surfaces *Adv.*

Funct. Mater. 25 1499–505

[22] Cheung E and Sitti M 2008 Adhesion of Biologically Inspired Oil-Coated Polymer Micropillars *J. Adhes. Sci. Technol.* 22 569–89

[23] Varenberg M and Gorb S A 2008 beetle-inspired solution for underwater adhesion *J. R. Soc. Interface* 5 383–5

[24] Xue L, Kovalev A, Eichler-Volf A, Steinhart M and Gorb S N 2015 Humidity-enhanced wet adhesion on insect-inspired fibrillar adhesive pads *Nature Communications* 6 6621

[25] Gong L, Yu H, Li R, Wang C, Jia H and Wang X 2016 Morphology and adhesion mechanisms of newt *Cynops orientalis*' foot pads (in Chinese) *Chin. Sci. Bull.* 61 2587–95

[26] Wang S, Li M, Huang W and Wang X 2016 Sticking/climbing ability and morphology studies of the toe pads of Chinese fire belly Newt *J. Bionic. Eng.* 13 115–23

[27] Huang W and Wang X 2013 Biomimetic design of elastomer surface pattern for friction control under wet conditions *Bioinspiration & Biomimetics* 8 046001

[28] Labonte D and Federle W 2015 Scaling and biomechanics of surface attachment in climbing animals *Philos. T. R. Soc. B.* 370 20140027

[29] Stark A Y, Badge I, Wucinich N A, Sullivan T W, Niewiarowski P H and Dhinojwala A 2013 Surface wettability plays a significant role in gecko adhesion underwater *PNAS* 110 6340–5

[30] Ba-Omar T A, Downie J R and Barnes W J P 2000 Development of adhesive toe-pads in the tree-frog (Phyllomedusa trinitatis) *Journal of Zoology* 250 267–82

[31] Arzt E, Gorb S and Spolenak R 2003 From micro to nano contacts in biological attachment devices *Proc. Nati. Acad. Sci.* 100 10603–6

[32] Johnson K L 1998 Mechanics of Adhesion *Tribol. Int.* 31 413–418

[33] Makhovskaya Y Y and Goryacheva I G 1999 The combined effect of capillarity and elasticity in contact interaction *Tribol. Int.* 32 507–15

[34] Defante A P, Burai T N, Becker M L and Dhinojwala A 2015 The Consequences of Water Between Two Hydrophobic Surfaces on Adhesion and Wetting *Langmuir* 31 2398-406

[35] Jung Y C and Bhushan B 2006 Contact angle, adhesion, and friction properties of micro- and nanopatterned polymers for superhydrophobicity *Nanotechnology* 17 4970–80

[36] Kaveh F, Ally J, Kappl M and Butt H J 2014 Hydrodynamic force between a sphere and a soft, elastic surface *Langmuir* 30 11619–24

[37] Dhong C and Frechette J 2015 Coupled effects of applied load and surface structure on the viscous forces during peeling *Soft Matter* 11 1901-10

[38] Kovalev A E, Filippov A E and Gorb S N 2013 Insect wet steps: loss of fluid from insect feet adhering to a substrate *J. R. Soc. Interface* 10 20120639

[39] Patil S, Mangal R, Malasi A and Sharma A 2012 Biomimetic wet adhesion of viscoelastic liquid films anchored on micropatterned elastic substrates *Langmuir* 28 14784–91